SCIENTIFIC REPORTS

OPEN

SUBJECT AREAS:
INORGANIC CHEMISTRY
MATERIALS CHEMISTRY

Received
17 October 2013

Accepted
27 November 2013

Published
12 December 2013

Correspondence and requests for materials should be addressed to K.-X.W. (k.wang@sjtu.edu.cn) or J.-S.C. (chemcj@sjtu.edu.cn)

Hierarchical $Li_4Ti_5O_{12}/TiO_2$ composite tubes with regular structural imperfection for lithium ion storage

Yan-Mei Jiang, Kai-Xue Wang, Hao-Jie Zhang, Jing-Feng Wang & Jie-Sheng Chen

School of Chemistry and Chemical Engineering, Shanghai Jiao Tong University, Shanghai 200240, China.

Hierarchical $Li_4Ti_5O_{12}/TiO_2$ tubes composed of ultrathin nanoflakes have been successfully fabricated via the calcination of the hydrothermal product of a porous amorphous TiO_2 precursor and lithium hydroxide monohydrate. The hierarchical tubes are characterized by powder X-ray diffraction, nitrogen adsorption/desorption, scanning electron microscopy and transmission electron microscopy techniques. These nanoflakes exhibit a quite complex submicroscopic structure with regular structural imperfection, including a huge number of grain boundaries and dislocations. The lithium ion storage property of these tubes is evaluated by galvanostatic discharge/charge experiment. The product shows initial discharge capacities of 420, 225, and 160 mAh g^{-1} at 0.01, 0.1, and 1.0 A g^{-1}, respectively. After 100 cycles, the discharge capacity is 139 mAh g^{-1} at 1.0 A g^{-1} with a capacity retention of 87%, demonstrating good high-rate performance and good cycleability. The high electrochemical performance is attributed to unique structure and morphology of the tubes. The regular structural imperfection existed in the nanoflakes also benefit to lithium ion storage property of these tubes. The hierarchical $Li_4Ti_5O_{12}/TiO_2$ tubes are a promising anode material for lithium-ion batteries with high power and energy densities.

Rechargeable lithium ion batteries have been successfully adopted as power sources for portable electronic devices because of their high energy density and long cycle life[1], whereas the practical application of lithium ion batteries to (hybrid) electric vehicles and stationary electric energy storage largely depends on the electrochemical performance of the electrode materials, such as large specific capacities, high rate capability and good cycling stability. It is envisaged that the introduction of a nanostructure and the increase of crystallographic defect concentration and grain boundary (GB) density are feasible strategies to improve the electrochemical performance of electrode materials. Nanostructured materials with small particle size and large specific surface area can provide relatively shortened mass and charge transport pathways and charming surface activities, resulting in enhanced rate capabilities[2].

The research on structural imperfection derived from crystallographic defects is a very active and rapidly developing area in solid-state chemistry[3]. Crystallographic defects can bring forth rich structural chemistry and unexpected properties to the crystalline materials. For example, the smooth mass transfer in a solid-state reaction can be achieved only when the reactants have certain defect concentration. Oxygen-deficient ferrites with a spinel structure can efficiently decompose CO_2 into carbon through the transfer of oxygen to the oxygen vacancies[4]. The presence of defects in the crystal structures may enhance the lithium ion transport properties and electronic conductivity of the electrode materials[5–13]. Therefore, it is promising to enhance the rate performance of lithium ion batteries to a great extent by introducing defects to the electrode materials.

A large number of lithium ions can be stored on the interfacial area of the nanostructured materials with a high grain boundary density, increasing the specific capacities of these materials[14,15]. It is of interest that the capacity introduced by the interfacial lithium storage is almost independent on the charge-discharge rate due to its thermodynamic characteristics[16,17]. Dual- and multi-phase materials are expected to provide increased grain boundary density. Recently, the interface in dual-phase $Li_4Ti_5O_{12}/TiO_2$ materials is demonstrated to be superior for storing the extra lithium[18–21].

Herein, the synergistic effect of nanostructure, crystallographic defect and grain boundary on the lithium ion storage properties of electrode materials is observed for dual-phase hierarchical $Li_4Ti_5O_{12}/TiO_2$ tubes prepared via the calcination of a lithium titanium oxide hydrate, which is the hydrothermal product of a porous amorphous TiO_2 precursor and lithium hydroxide monohydrate. The hierarchical tubes are composed of ultrathin nanoflakes with an ordered defect structure. Plenty of grain boundaries are present within the $Li_4Ti_5O_{12}$ crystallites,

and among $Li_4Ti_5O_{12}$ and TiO_2 crystallites in the nanoflakes. These hierarchical tubes exhibit large reversible capacities and good cycling performance.

Results

The X-ray diffraction (XRD) pattern of the produced tubes is shown in Figure 1a The broadened peaks located at 18.44°, 35.59°, 43.40°, and 62.92° can be readily indexed to the (111), (311), (400), and (440) diffractions, respectively, of $Li_4Ti_5O_{12}$ with a cubic spinel structure (JCPDS No. 49-0207). The additional peaks at 25.34°, 38.03°, 47.99°, 54.25°, and 55.04° are ascribed to the (101), (004), (200), (105), and (211) diffractions, respectively, of anatase TiO_2 (JCPDS No. 21-1272). The XRD analysis indicates that both spinel $Li_4Ti_5O_{12}$ and anatase TiO_2 exist in the sample obtained, generating a dual-phase $Li_4Ti_5O_{12}/TiO_2$ composite material. The anatase TiO_2 may arise from the crystallization of residual amorphous titania surviving the hydrothermal treatment. The content of spinel $Li_4Ti_5O_{12}$ in the composite is approximately 64 wt% based on the XRD analysis. The morphology of the $Li_4Ti_5O_{12}/TiO_2$ composite is revealed by SEM and TEM observation (Figure 1b, c). The $Li_4Ti_5O_{12}/TiO_2$ exhibits a tube-like morphology assembled by interleaving ultrathin nanoflakes. The diameter of the tubes ranges from 0.5 to 2.0 μm with a length of 5–20 μm. The nanoflakes with a smooth surface are approximately 1 μm in length and 200–400 nm in width. As observed in the TEM image, plenty of void space exists among the nanoflakes, forming a three-dimensional (3D) channel system which facilitates the transportation of the electrolyte and lithium ions. The inner side of the nanoflakes is fused together to form the wall of the tubes, ensuring the good electronic contact of these flakes.

Figure 2 shows further structural feature of the hierarchical $Li_4Ti_5O_{12}/TiO_2$ tubes. A schematic illustration of the individual nanoflake is drawn to show the regions revealed by the HRTEM observation (Figure 2a). The HRTEM image of the nanoflake taken in region **I** clearly exhibits a periodic arrangement of fringes with an average distance of approximately 1.7 nm, obviously larger than the lattice fringe spacings of $Li_4Ti_5O_{12}$ and TiO_2 (Figure 2b). The lattice-fringe-like periodic pattern is believed to be derived from defects, demonstrating the regular structural imperfection of these nanoflakes. However, the corresponding selected area electron diffraction (SAED) (inset in Figure 2b) along the [011] zone axis (perpendicular to the nanoflake surface) exhibits a series of spot pattern, characteristic for a single-crystal-like structure. All of the diffraction spots can be well indexed to the spinel $Li_4Ti_5O_{12}$ with a cubic structure in which the direction [hkl] is perpendicular to the (hkl) plane. Therefore, it can be concluded that the $Li_4Ti_5O_{12}$ nanoflakes are bound by (011) facets on both the top and bottom surfaces. The HRTEM images (Figure 2c, d) of the nanoflake in region **I** and **II** are taken along the direction that almost parallels with the nanoflake plane. As shown in Figure 2c, the lattice fringes with a spacing of 0.50 nm attributing to the (111) plane of spinel $Li_4Ti_5O_{12}$ with a lattice fluctuation are clearly observed. A careful examination of the HRTEM image indicates that structural imperfection is derived from the interlacing of two or three closely packed parallel (111) planes. This layer-by-layer-like stacking can be clearly observed in the TEM images viewing along or perpendicular to the surface of the nanoflakes (Figure 2d, e). The interlayer spacing of the lattice-fringe-like structural imperfection is approximately 1.7 nm, consistent with that observed in Figure 2b. For a cubic structure, the dihedral angle between the (111) planes is 70.5°. Distinct lattice fringes with a distance of approximately 0.48 nm are observed, corresponding to the (111) planes of spinel $Li_4Ti_5O_{12}$ (Figure 2e). The angle between these lattice fringes is approximately 70.5°, consistent with the cubic structure of $Li_4Ti_5O_{12}$. It is interesting that plenty of grain boundaries exist among the crystalline domains in the nanoflakes (Figure 2f).

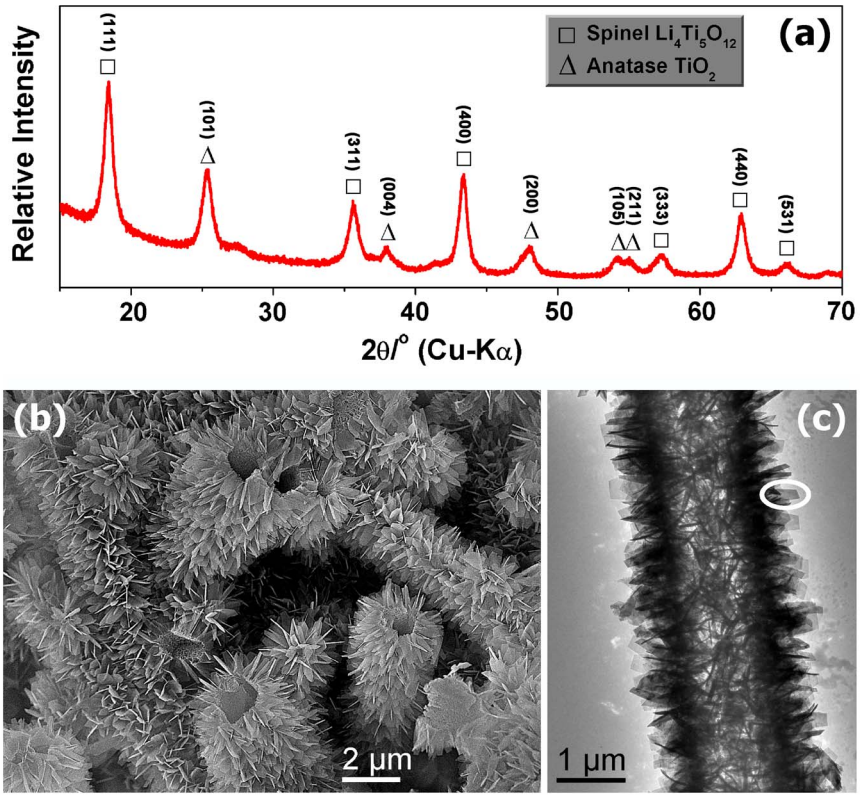

Figure 1 | X-ray diffraction pattern and microscopy images of the hierarchical $Li_4Ti_5O_{12}/TiO_2$ tubes. (a) X-ray diffraction pattern of the hierarchical tubes, indicating that both spinel $Li_4Ti_5O_{12}$ and anatase TiO_2 exist in the sample obtained. (b) SEM image shows that a tube-like morphology assembled by interleaving ultrathin nanoflakes. (c) TEM image of the hierarchical $Li_4Ti_5O_{12}/TiO_2$ tubes with an individual nanoflake indicated in the white circle.

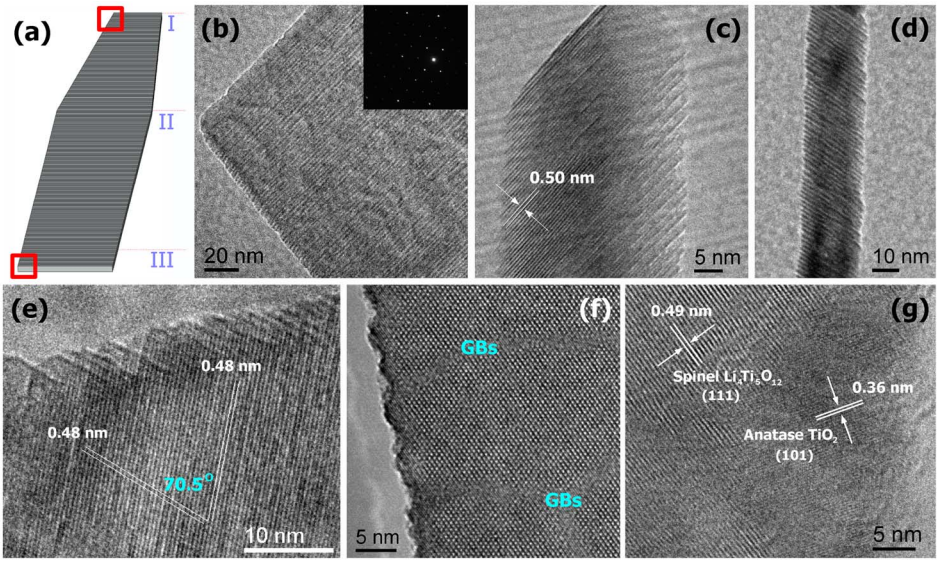

Figure 2 | Schematic drawing and electron microscopy images of the nanoflake. (a) Schematic representation of a structural model of the nanoflake, showing a regular lamellar structure with defects. (b, c) High resolution TEM (HRTEM) images of the nanoflake in region I. Regular structural imperfection with an average distance of approximately 1.7 nm is clearly observed in the TEM image (b). In the SAED pattern inset in b, the electron diffraction along the [011] zone axis (perpendicular to the nanoflake surface) is indexed to the cubic structure of spinel $Li_4Ti_5O_{12}$, each stacked layer are offset and stepping upwards layer by layer like a staircase (c). (d, e, f) HRTEM images of the nanoflake in region II. The layers stacked in the nanoflakes form a dihedral angel {111} vs. {111} of approximately 70.5°, consistent with the cubic structure of $Li_4Ti_5O_{12}$. Grain boundaries and dislocations present in the nanoflakes (f). (g) HRTEM image of the nanoflake in region III, confirming the co-existence of the spinel $Li_4Ti_5O_{12}$ and anatase TiO_2.

These attractive grain boundaries are expected to provide extra diffusion path and storage sites for lithium ions. Figure 2g shows the HRTEM image taken in region **III**, the root section of the nanoflake. The lattice fringe spacings of 0.49 and 0.36 nm observed are ascribed to the (111) plane of spinel $Li_4Ti_5O_{12}$ and (101) plane of anatase TiO_2, respectively, confirming the co-existence of the spinel $Li_4Ti_5O_{12}$ and anatase TiO_2. In addition, a great deal of grain boundaries among the spinel $Li_4Ti_5O_{12}$ and anatase TiO_2 are also observed in the region. The HRTEM observation is in agreement with that of the XRD analysis. The presence $Li_4Ti_5O_{12}$ and TiO_2 dual phase significantly increases the grain boundary density.

The textural feature of the hierarchical $Li_4Ti_5O_{12}/TiO_2$ tubes is characterized by nitrogen adsorption/desorption measurements (Supplementary Figure 1). The isotherms are identified as of type IV with an H3 hysteresis loop, indicating the presence of slit-like pores. This is consistent with the SEM and TEM observation. A hysteresis loop with a sharp capillary condensation is presented at a relative pressure of 0.80 to 0.97, which is due to the existence of macroporous structures. The pore size distribution shows feature characteristic for hierarchical materials. The specific Brunauer-Emmett-Teller (BET) surface area and the pore volume are determined to be 107 $m^2\ g^{-1}$ and 0.52 $cm^3\ g^{-1}$, respectively.

Cyclic voltammetry (CV) was used to investigate the electrochemical behavior of the hierarchical $Li_4Ti_5O_{12}/TiO_2$ tubes with regular structural imperfection. Figure 3 shows the CV curves of the hierarchical $Li_4Ti_5O_{12}/TiO_2$ tubes at a scan rate of 0.2 mV s^{-1} in the potential range from 2.5 to 1.0 V. In the first cycle, three pairs of peaks were observed. Two pairs of cathodic/anodic peaks located at 1.43/1.65 V, and 1.64/2.06 V versus Li^+/Li are associated with lithium ion insertion/extraction within the spinel $Li_4Ti_5O_{12}$ and anatase TiO_2 lattices, respectively. An extraordinary pair of peaks located at 1.27/1.78 V versus Li^+/Li are distinctly observed, denoted as *S* peaks. It is generally accepted that the *S* peaks are related to the surface-confined charge-transfer processes with the presence of amorphous phase in the organized skeleton[22,23]. The *S* peaks have been well documented in the literature to explain the electrochemical behavior of Ti-based compounds, such as TiO_2 (B)[24], anatase[22], spinel $Li_4Ti_5O_{12}$[25], dual-phase $Li_4Ti_5O_{12}$–TiO_2[18], and layered hydrogen titanate[26]. For the hierarchical $Li_4Ti_5O_{12}/TiO_2$ tubes, the appearance of *S* peaks is attributed to the presence of the regular structural imperfection in the nanoflakes. In the following cycle, the peak potentials of insertion and extraction in/from spinel $Li_4Ti_5O_{12}$ lattices process slightly shift to 1.46 and 1.66 V, respectively, and the pair of peaks corresponding to the $TiO_2 - Li_xTiO_2$ redox couples almost disappears. It means that the electrode reaction of the hierarchical $Li_4Ti_5O_{12}/TiO_2$ tubes is controlled by a mixed process of the faradaic pseudocapacitive and diffusion-limited reaction, benefiting performance enhancement of electrode active materials[18,25,27].

The electrochemical performance of the hierarchical $Li_4Ti_5O_{12}/TiO_2$ tubes was evaluated by galvanostatic charge-discharge technique. Figure 4a displays the initial three discharge/charge curves of the hierarchical $Li_4Ti_5O_{12}/TiO_2$ tubes at a current density of 0.01 A g^{-1} in the potential window of 2.5–1.0 V (versus Li^+/Li). In

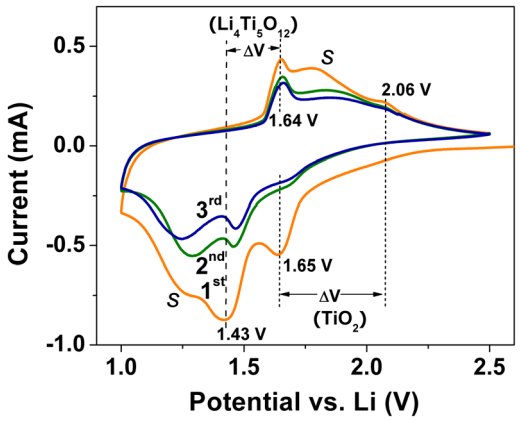

Figure 3 | Cyclic voltammogram of the hierarchical $Li_4Ti_5O_{12}/TiO_2$ tubes between 2.5 and 1.0 V with a scan rate of 0.2 mV s^{-1}. The unusually *S* peaks recorded are attributed to the presence of the regular structural imperfection in the nanoflakes.

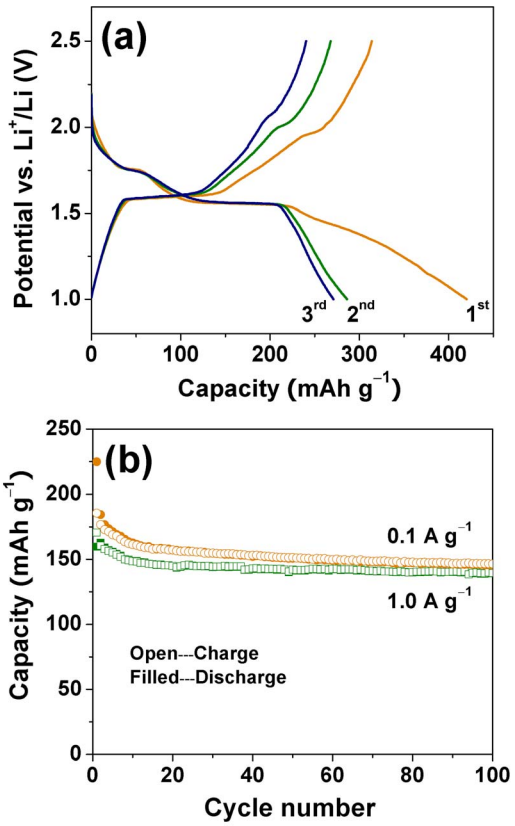

Figure 4 | Electrochemical characterizations of the hierarchical $Li_4Ti_5O_{12}/TiO_2$ tubes. (a) The initial three discharge/charge curves of the hierarchical $Li_4Ti_5O_{12}/TiO_2$ tubes at 0.01 A g^{-1}. (b) Cycling performance of the hierarchical $Li_4Ti_5O_{12}/TiO_2$ tubes at 0.1 and 1.0 A g^{-1}. The electrochemical evaluation suggests the large specific capacity, high rate capability and excellent cycling stability of these hierarchical tubes.

the discharge process, two potential plateaus at potentials of approximately 1.75 and 1.55 V are clearly observed. The first plateau at 1.75 V is ascribed to the phase transition from anatase TiO_2 to orthorhombic Li_xTiO_2 upon lithium ion insertion. The plateau at 1.55 V is attributed to the generation of a rocksalt-structured $Li_7Ti_5O_{12}$, resulting from the lithium ion insertion into the spinel $Li_4Ti_5O_{12}$. A long sloped region observed from 1.55 to 1.0 V can be assigned to the pseudocapacitive lithium storage behavior of the $Li_4Ti_5O_{12}/TiO_2$ tubes, characteristic of the electrochemical reactions involving surface-confined charge-transfer or interfacial storage processes[14–16,25]. At 0.01 A/g, the discharge capacity of the first cycle can reach a high lithiation capacity of 420 mAh g^{-1} and a de-lithiation capacity of 315 mAh g^{-1}. The discharge capacities of the second and third cycles are approximately 286 and 271 mAh g^{-1}, respectively, with the coulombic efficiency significantly improved. The initial discharge capacity of the hierarchical $Li_4Ti_5O_{12}/TiO_2$ tubes at 0.01 A g^{-1} (approximately C/16) is much higher than that of the nanostructured $Li_4Ti_5O_{12}$ at even lower current density (approximately 228 mAh g^{-1} at C/24)[28]. As revealed by the TEM observed, the grain boundary density of the $Li_4Ti_5O_{12}/TiO_2$ tubes can be significantly increased by introducing TiO_2 crystallites into the nanoflakes. Thus, the high specific capacity of the $Li_4Ti_5O_{12}/TiO_2$ tubes is mainly attributed to the extra amount of lithium ions stored on the interfacial area of the crystalline $Li_4Ti_5O_{12}$ and TiO_2 grains. In addition, the electrochemical properties of lithium ion insertion/extraction largely depend on the crystal surface plane orientation of the electrode materials. The lowest energy (011) surface of $Li_4Ti_5O_{12}$ is predicted to be energetically favorable for lithium ion insertion into the vacant 16*c* sites[29]. But for $Li_4Ti_5O_{12}$ nanoflakes with nearly 100% exposed (011) facets, the intercalation of lithium ions into empty tetrahedral 8*a* sites in the near surface region is not feasible. Thus, the extra charge capacity must result from the insertion of lithium ions into the ordered defect layers in spinel $Li_4Ti_5O_{12}$.

Cycling performance of the hierarchical $Li_4Ti_5O_{12}/TiO_2$ tubes at the discharge/charge current density of 0.1 and 1.0 A g^{-1} is shown in Figure 4b. Cycled at 0.1 A g^{-1}, a reversible capacity of 146 mAh g^{-1} is observed for the 100th cycle, giving a capacity retention rate of approximately 65%. Cycled at a current density of 1.0 A g^{-1}, the hierarchical $Li_4Ti_5O_{12}/TiO_2$ tubes show a discharge capacity of 160 mAh g^{-1} in the first cycle. Good capacity retention is realized over extended cycling. A charge capacity of 139 mAh g^{-1}, approximately 87% of its initial charge capacity is retained after 100 cycles. After 800 cycles, the discharge capacity of the hierarchical $Li_4Ti_5O_{12}/TiO_2$ tubes is still of 134 mAh g^{-1} (Supplementary Figure 2b). The cycling stability for the hierarchical $Li_4Ti_5O_{12}/TiO_2$ tubes at a large current density is distinctly superior to those for the related composite materials described in the literature[18–21]. Thus, the high cycling stability of the $Li_4Ti_5O_{12}/TiO_2$ tubes is mainly ascribed to their unique hierarchical tubular structure built up by thin nanoflakes.

The high specific capacity, good cycleability of the hierarchical $Li_4Ti_5O_{12}/TiO_2$ tubes constructed by nanoflakes are attributed to the synergistic effect of the hierarchical nanostructure, the ordered fringe-like crystallographic defect and the large number of grain boundaries among the spinel $Li_4Ti_5O_{12}$ and anatase TiO_2 nanocrystals. First, the 3D porous channel system of the composite material facilitates the transport of electrolyte and lithium ions within the electrode and the small thickness of the nanoflakes shortens the diffusion distance for both electron and lithium ions. Second, the fringe-like structural imperfection, abundant grain boundaries and phase interfaces in the hierarchical $Li_4Ti_5O_{12}/TiO_2$ composite favor the storage of extra lithium ions, increasing the specific capacity of the composite material. In addition, the abundant phase interfaces are also favorable for the fast electrochemical lithium-ion insertion and extraction processes, improving the kinetics of the electrode. Third, the tubular structure and thin nanoflakes effectively buffer the stress induced during the discharge/charge process, contributing to the cycling performance improvement of the composite. Because of these structural features, the hierarchical $Li_4Ti_5O_{12}/TiO_2$ composite exhibits large specific capacities and good cycling stability.

In summary, hierarchical $Li_4Ti_5O_{12}/TiO_2$ tubes composed of nanoflakes have been successfully fabricated through the conversion of a lithium titanium oxide hydrate upon calcination at 400°C. The structural imperfection formed in the nanoflakes during the phase transformation from lithium titanium oxide hydrate to spinel $Li_4Ti_5O_{12}$ has proved to be advantageous for lithium ion storage of these tubes. The obtained hierarchical $Li_4Ti_5O_{12}/TiO_2$ tubes exhibit a high initial discharge capacity of 420 mAh g^{-1} at 0.01 A g^{-1}. Cycling at 1.0 A g^{-1}, a capacity of 139 mAh g^{-1} is retained even after 100 cycles, indicating good cycling stability. The high electrochemical performance of the tubes is attributed to their unique nanostructure, including the 3D porous channel system, the structural imperfection in $Li_4Ti_5O_{12}$ nanoflakes and the high grain boundary density among the nanoparticles. The 3D porous channel system facilitates the mass transport of the electrolyte and lithium ions and provides sufficient void space to accommodate the volume change during the discharge/charge process, ensuring the good cycling performance. Such elaborate combination of crystal structure and architectural mode could be helpful for designing new high rate composite electrodes.

Methods

Preparation of hierarchical $Li_4Ti_5O_{12}/TiO_2$ tubes. The hierarchical $Li_4Ti_5O_{12}/TiO_2$ tubes were prepared from a porous amorphous TiO_2 as precursor by a hydrothermal process and subsequent calcination. Typically, titanium glycolate was first synthesized via heating the mixture of ethylene glycol and tetrabutyl titanate (1 : 100 by volume) at 160°C for 2 h under vigorous stirring. The porous amorphous TiO_2 were prepared through the irradiation of titanium glycolate under ultraviolet light

(Supplementary Figure 3a–b). A mixture of the amorphous titania (240 mg, 3.00 mmol) and lithium hydroxide monohydrate (111 mg, 2.65 mmol) was added to 24 mL of ditilled water with continuous stirring. The obtained suspension was transferred into a 30 mL Teflon-lined stainless-steel autoclave, which was then heated at 130°C for 7 d. The white precipitate of layered hydrous lithium titanate was collected by filtration, washed with ethanol thoroughly, and dried naturally at room temperature (Supplementary Figure 3c–d). The final product of hierarchical $Li_4Ti_5O_{12}/TiO_2$ tubes was generated by the calcination of the layered hydrous lithium titanate at 400°C for 1.5 h.

Characterization. Powder X-ray diffraction (XRD) patterns were recorded on a Rigaku Dmax-2200 diffractometer (Rigaku, Japan) with Cu Kα radiation ($\lambda = 1.5418$ Å). The morphology of the sample was observed with a scanning electron microscope (SEM, JSM-7401F, JEOL, Japan). The microstructure of the sample was characterized by using transmission electron microscope (TEM, JEM-2100F, JEOL, Japan) and high resolution transmission electron microscope (HRTEM, JEM-2100F, JEOL, Japan), operating at 200 kV. The specific surface areas of the samples were measured on a Micromeritics ASAP 2010 M + C nitrogen adsorption instrument (Micrometritices Inc., USA) at 77 K.

Electrochemical properties of the hierarchical $Li_4Ti_5O_{12}/TiO_2$ tubes were evaluated with CR2016 coin cells. The working electrode was prepared on an aluminum foil by using a doctor-blade method with a slurry composed of 75 wt.% active materials (TiO_2), 15 wt.% conductivity agent (acetylene black), and 10 wt.% binder (polyvinylidene fluoride, PVDF). Lithium metal foil was used as both the counter and reference electrodes. A microporous polypropylene membrane (Celgard 2500) was used as the separator. Coin cells were assembled in an argon filled glove box with both moisture and oxygen contents below 1.0 ppm. The electrolyte was 1.0 M of $LiClO_4$ in ethylene carbonate/dimethyl carbonate (EC/DEC, 1 : 1 by volume). The galvanostatic charge and discharge experiment was performed with a battery tester LAND-CT2001A in the voltage range of 1.0–2.5 V at room temperature. Cyclic voltammograms (CV) measurement was conducted by using an electrochemical cell with a three-electrode configuration. Li metal foil was selected as the reference and counter electrode. The electrolyte was 1 M $LiClO_4$ in ethylene carbonate/dimethyl carbonate (EC/DEC, 1 : 1 by volume). The cyclic voltammograms (CV) were conducted on a CHI 660B electrochemical workstation at a scanning rate of 0.2 mV s^{-1} in a potential range of 2.5–1.0 V (vs Li^+/Li).

1. Tarascon, J. M. & Armand, M. Issues and challenges facing rechargeable lithium batteries. *Nature* **414**, 359–367 (2001).
2. Bruce, P. G., Scrosati, B. & Tarascon, J. M. Nanomaterials for Rechargeable Lithium Batteries. *Angew. Chem. Int. Ed.* **47**, 2930–2946 (2008).
3. West, A. R. *Solid State Chemistry and its Applications* (J. Wiley & Sons, Chichester, 1984).
4. Nordhei, C., Mathisen, K., Safonova, O., van Beek, W. & Nicholson, D. G. Decomposition of Carbon Dioxide at 500°C over Reduced Iron, Cobalt, Nickel, and Zinc Ferrites: A Combined XANES–XRD Study. *J. Phys. Chem. C* **113**, 19568–19577 (2009).
5. Badi, S. P. *et al.* Direct synthesis of nanocrystalline $Li_{0.90}FePO_4$: observation of phase segregation of anti-site defects on delithiation. *J. Mater. Chem.* **21**, 10085–10093 (2011).
6. Chung, S. Y., Choi, S. Y., Yamamoto, T. & Ikuhara, Y. Atomic-Scale Visualization of Antisite Defects in $LiFePO_4$. *Phys. Rev. Lett.* **100**, 125502 (2008).
7. Gibot, P. *et al.* Room-temperature single-phase Li insertion/extraction in nanoscale Li_xFePO_4. *Nat. Mater.* **7**, 741–747 (2008).
8. Hamelet, S. *et al.* Existence of Superstructures Due to Large Amounts of Fe Vacancies in the $LiFePO_4$-Type Framework. *Chem. Mater.* **23**, 32–38 (2010).
9. Janssen, Y., Middlemiss, D. S., Bo, S. H., Grey, C. P. & Khalifah, P. G. Structural Modulation in the High Capacity Battery Cathode Material $LiFeBO_3$. *J. Am. Chem. Soc.* **134**, 12516–12527 (2012).
10. Lee, J., Zhou, W., Idrobo, J. C., Pennycook, S. J. & Pantelides, S. T. Vacancy-Driven Anisotropic Defect Distribution in the Battery-Cathode Material $LiFePO_4$. *Phys. Rev. Lett.* **107**, 085507 (2011).
11. Luo, J. Y., Chen, L. J., Zhao, Y. J., He, P. & Xia, Y. Y. The effect of oxygen vacancies on the structure and electrochemistry of $LiTi_2(PO_4)_3$ for lithium-ion batteries: A combined experimental and theoretical study. *J. Power Sources* **194**, 1075–1080 (2009).
12. Wang, Y. *et al.* Defect effects on the physical and electrochemical properties of nanoscale $LiFe_{0.92}PO_4$ and $LiFe_{0.92}PO_4$/C/graphene composites. *Nanoscale* **5**, 3704–3712 (2013).
13. Zheng, J. *et al.* Enhanced Li^+ ion transport in $LiNi_{0.5}Mn_{1.5}O_4$ through control of site disorder. *Phys. Chem. Chem. Phys.* **14**, 13515–13521 (2012).
14. Guo, X. *et al.* Capacitive Energy Storage on Fe/Li_3PO_4 Grain Boundaries. *J. Phys. Chem. C* **115**, 3803–3808 (2011).
15. Yu, X. Q. *et al.* Reversible lithium storage in LiF/Ti nanocomposites. *Phys. Chem. Chem. Phys.* **11**, 9497–9503 (2009).
16. Jamnik, J. & Maier, J. Nanocrystallinity effects in lithium battery materials - Aspects of nano-ionics. Part IV. *Phys. Chem. Chem. Phys.* **5**, 5215–5220 (2003).
17. Maier, J. Nanoionics: ion transport and electrochemical storage in confined systems. *Nat. Mater.* **4**, 805–815 (2005).
18. Li, X., Lai, C., Xiao, C. W. & Gao, X. P. Enhanced high rate capability of dual-phase $Li_4Ti_5O_{12}$-TiO_2 induced by pseudocapacitive effect. *Electrochim. Acta* **56**, 9152–9158 (2011).
19. Rahman, M. M. *et al.* Basic molten salt process A new route for synthesis of nanocrystalline $Li_4Ti_5O_{12}$-TiO_2 anode material for Li-ion batteries using eutectic mixture of $LiNO_3$-LiOH-Li_2O_2. *J. Power Sources* **195**, 4297–4303 (2010).
20. Rahman, M. M., Wang, J. Z., Hassan, M. F., Wexler, D. & Liu, H. K. Amorphous Carbon Coated High Grain Boundary Density Dual Phase $Li_4Ti_5O_{12}$-TiO_2: A Nanocomposite Anode Material for Li-Ion Batteries. *Adv. Energy Mater.* **1**, 212–220 (2011).
21. Wang, J. *et al.* $Li_4Ti_5O_{12}$–TiO_2 composite anode material for lithium-ion batteries. *J. Power Sources* **222**, 196–201 (2013).
22. Kavan, L., Rathousky, J., Gratzel, M., Shklover, V. & Zukal, A. Surfactant-templated TiO_2 (anatase): Characteristic features of lithium insertion electrochemistry in organized nanostructures. *J. Phys. Chem. B* **104**, 12012–12020 (2000).
23. Kavan, L., Rathousky, J., Gratzel, M., Shklover, V. & Zukal, A. Mesoporous thin film TiO_2 electrodes. *Microporous and Mesoporous Mater.* **44**, 653–659 (2001).
24. Zukalova, M., Kalbac, M., Kavan, L., Exnar, I. & Graetzel, M. Pseudocapacitive lithium storage in TiO_2(B). *Chem. Mater.* **17**, 1248–1255 (2005).
25. Lai, C., Dou, Y. Y., Li, X. & Gao, X. P. Improvement of the high rate capability of hierarchical structured $Li_4Ti_5O_{12}$ induced by the pseudocapacitive effect. *J. Power Sources* **195**, 3676–3679 (2010).
26. Li, J. R., Tang, Z. L. & Zhang, Z. T. Layered hydrogen titanate nanowires with novel lithium intercalation properties. *Chem. Mater.* **17**, 5848–5855 (2005).
27. Kavan, L. *et al.* Lithium storage in nanostructured TiO_2 made by hydrothermal growth. *Chem. Mater.* **16**, 477–485 (2004).
28. Chiu, H. c. *et al.* Aqueous Synthesized Nanostructured $Li_4Ti_5O_{12}$ for High-Performance Lithium Ion Battery Anodes. *J. Electrochem. Soc.* **160**, A3041–A3047 (2013).
29. Ganapathy, S. & Wagemaker, M. Nanosize Storage Properties in Spinel $Li_4Ti_5O_{12}$ Explained by Anisotropic Surface Lithium Insertion. *ACS Nano* **6**, 8702–8712 (2012).

Acknowledgments

This work was financially supported by the National Basic Research Program (2013CB934102, 2011CB808703) and the National Natural Science Foundation of China.

Author contributions

Y.J. and K.W. developed the idea and designed the experiments. Y.J. performed the sample fabrication, measurements and data analysis. Y.J. and H.Z. performed the electrochemical experiments. Y.J., K.W., H.Z., J.W. and J.C. analyzed the data, and discussed the results. Y.J., K.W. and J.C. co-wrote the paper.

Additional information

Supplementary information accompanies this paper at http://www.nature.com/scientificreports

Competing financial interests: The authors declare no competing financial interests.

How to cite this article: Jiang, Y.-M., Wang, K.-X., Zhang, H.-J., Wang, J.-F. & Chen, J.-S. Hierarchical $Li_4Ti_5O_{12}/TiO_2$ composite tubes with regular structural imperfection for lithium ion storage. *Sci. Rep.* **3**, 3490; DOI:10.1038/srep03490 (2013).